

Blue Ridge Wind Collaborative

Prototype Development Report Collegiate Wind Competition 2024

Prototype Development Team

Jaedyn Williams	Senior Technical Lead
Henry Thompson	Mechanical Lead
Jackson Andrew	Power Systems Lead
Puneeth Vangumalla	Controls Lead
Silas Nickerson	Aerodynamics Co-Lead
Yates Kirby	Aerodynamics Co- Lead

Power Systems & Controls

Yigit Kaya	Alec Crispino
Aditya Rao	Reve Meili
Scott Miloy	Makeda Solomon
Theodore Moss	Daniel Befekadu
Tom Dagget	Walter Lin
Juan Martinez-Medina	Timothy Estrada
Josh Grubb	Sammy Craypoff
Anthony Concessi	

Aerodynamics

Quinn McIver
River Hamme

Mechanical

Alden Wathen
Ayah Ali
Ben Dye
Carolyn North
Dane Barnes
Matthew Lewis

Jack Stevens
Jodh Singh
Kate Douglas
Marisa Gibbs
Nick Landicho
Sabin Constantinescu

Faculty Advisors

Dr. Nanyaporn Intaratep Aerospace & Ocean Engineering
Dr. Arthur Ball Collegiate Assistant Professor,
Bradley Department of Electrical &
Computer Engineering

Contents

- Executive Summary..... 2**
- Blade Design 2**
- Blade Fabrication 3**
- Blade Hub 5**
- Turbine Structures 6**
 - Yaw and Nacelle 7**
 - Design and Construction 8**
 - Testing..... 8**
 - Installation 11**
- Digitally Controllable Load..... 11**
- Generator..... 12**
- Turbine Side Electronics 13**
- Finite State Machine..... 13**
- Use of Legacy Parts 14**
- References..... 15**

Executive Summary

The goal of the Blue Ridge Wind Collaborative (BRWC), made up of students from Virginia Tech (VT) and James Madison University (JMU), was to create an efficient wind turbine prototype to enhance student learning of wind energy technology. This year, the team’s design objectives are to optimize the design of mechanical sub systems, research and manufacture optimal turbine blades, and create a reliable electrical system to successfully perform all tasks of the Collegiate Wind Competition 2024 (CWC). The team divided work into three subteams to achieve these goals, Power Systems and Controls (PSC), Mechanical, and Aerodynamics.

The PSC subteam designed the digitally controllable load (DCL). The DCL performs the MPPT algorithm by switching load resistors as wind speed changes. The team's turbine will also know its rated power and attempt to remain at that rated power at wind speeds greater than 11m/s by pitching and changing load resistance. The PSC team also chose an optimal generator for the competition’s scoring. The Mechanical subteam focused on reducing the size of the turbine’s systems while improving performance. Pitch control was simplified and made compact. The blade hub’s weight and size were reduced to improve cut in speed and allow for longer blades. A new mounting structure and nacelle was also developed. Foundation design further optimizes the foundation’s strength to weight ratio. The Aerodynamics subteam researched, designed, optimized, and manufactured blades. Low-Reynolds number airfoils were optimized with blade element momentum theory. Based on testing results, the team decided to use the SG6043 airfoil. The team pursued multiple methods of creating a hollow carbon fiber blade, but it could not be refined enough for a final product. Instead, wrapping the root in carbon fiber and using a printer that could embed onyx plastic with carbon fiber were both found to be viable solutions. With extensive testing, the onyx and carbon fiber blades proved to have the best power and consistency.

This report will discuss design improvements, justifications for designs, setbacks that the team encountered, and results from testing the prototype in the wind tunnel. The report will give an overview of the entire system and the interconnections between different components of the system.



Figure 1: Full Turbine Assembly

Blade Design

To begin blade design, the team researched papers on low Reynolds number airfoils [1][2] and airfoils suitable for small-scale wind turbines [3]. Using this information the team compiled a list of 12 airfoils, which were compared in a weighted decision matrix (Table 1). The four highlighted airfoils were selected as candidates for the final blade cross section. The SG6041 had the fourth highest score, but the SD2030 was chosen instead due to the similarity between the SG6041 and the SG6043.

To optimize the chord length and twist angle, an optimization code was written in MATLAB. The code used Betz optimum equations [4], which use the blade element momentum theory to take inertia into consideration, but neglect drag. An optimal chord and twist were found at multiple blade elements, and the blade was designed using QBlade software. Data from previous years was used to choose the design tip speed ratio (TSR). Airfoils that operated better at lower wind speeds were optimized at a TSR of 3, while the rest used a TSR of up to 5.

Table 1: Airfoil Decision Matrix

	Max Lift	Drag	L/D	Structure	Printability	Score
Weights	3	2	2.5	1	1.5	
s1210	5.4	5	2.2	0.6	0.8	33.5
GOE 79	3.6	7	8	5	2.2	53.1
Bergy BW-3	6.6	5	8.7	5.2	9	70.25
SG6043	8	3.6	7	7.4	9.1	69.75
SD2030	1.9	9	7	7.4	8	60.6
S822	1.8	3.2	0.8	8	0.6	22.7
A18	3.6	7.8	7.4	6	6.6	60.8
SD7043	5.2	6.6	7	7.4	4.2	60
FX 63-137	8.4	4	4	7	3	54.7
SG6041	7	3	6	7	8	61
s1223	9.4	4.8	5.6	6	6.8	68
e193	2.6	4.2	8	8	8	56.2

Optimized blade shapes from each airfoil were prototyped and tested in the open-jet wind tunnel. Test results displayed in Figure 2 indicated that the SG6043 blades produced highest power at wind speed of 5 to 11 m/s. The SD2030 blades showed promise at low wind speeds, but due to weight imbalances were not tested past 5 m/s. Also, the optimized chord was large enough at the root to interfere with the hub of the turbine, so the SD2030's were not considered to be the best choice. Therefore, the SG6043 blade design was chosen for use in the competition. The optimized SG6043 blade design featured a root-to-tip span of 21 cm, a maximum chord length of 5.7 cm and a maximum twist of 32°.

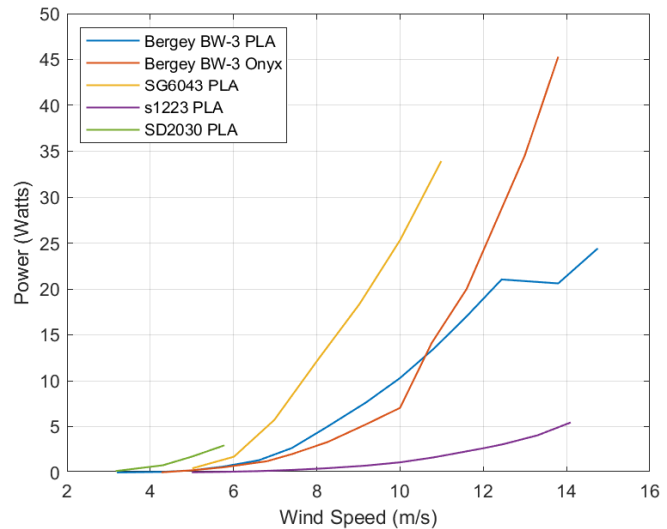


Figure 2: Airfoil Test Results

Blade Fabrication

Prototype testing blades were 3D printed in PLA plastic. This method allowed for quick production and modification. A full set of blades could be printed and ready to test in 18-22 hours. However, with PLA 3D printing there were structural and surface quality concerns, particularly with the uniformity of the trailing edge. To address the structural concerns of the PLA blades, 20% infill PLA SG6043 airfoil blades were tested with increasing wind speed until failure. At 14 m/s and 2528 RPM the blades experienced failure at the root, where the pin connects the blades to the hub. To increase the factor of safety at the root and to prevent failure during testing, the team decided to wrap each root with carbon fiber. This fabrication method allowed the team to



Figure 3: PLA blades with carbon fiber wrapped roots.

quickly produce a blade for aerodynamic testing, while eliminating the concerns of failure. The carbon fiber required 24 hours to cure, giving a total time of 42 to 46 hours to produce a full blade set. When the blades wrapped in carbon fiber were tested, they survived at 16.7 m/s and 3700 RPM, where the foundation began to experience failure.

To produce the optimal blade for the competition, the team pursued new fabrication methods of carbon fiber blades, both using a blade mold and a negative mold, and compared the results to the carbon fiber wrapped PLA blades. Initially, the results were promising, but many quality issues arose during the process, making the root wrapping method the most effective. From past years' experience, wrapping the root in carbon fiber is much easier to achieve than wrapping the whole blade. Another alternative fabrication solution was found by 3D printing the blades from a combination of onyx plastic

and carbon fiber using a Markforged FX-10 3D printer (Figure 4). This method had a longer lead time than PLA plastic, but had promising results with better tolerances, eliminating the jagged trailing edge (see Figure 3).

PLA blades with wrapped roots and the onyx/carbon fiber prints were compared over multiple performance trials in the wind tunnel. As shown in figure 6, the carbon fiber prints had more consistent results with a higher average power. This is likely due to the higher quality printer used for the blades and increased stiffness from the carbon fiber, leading to less variation during testing.

The final blade set was used to generate a non-dimensional coefficient of power vs tip speed ratio plot. The peak will shift with the resistance, but a resistance of 14.3 Ohms was used to most accurately represent what the turbine will undergo during an optimal test. Figure 5 shows a peak performance at a TSR of 4. This TSR is higher than previous years due to the reduced cord length of the blades used this year.



Figure 4: Carbon Fiber SG6043 Blades

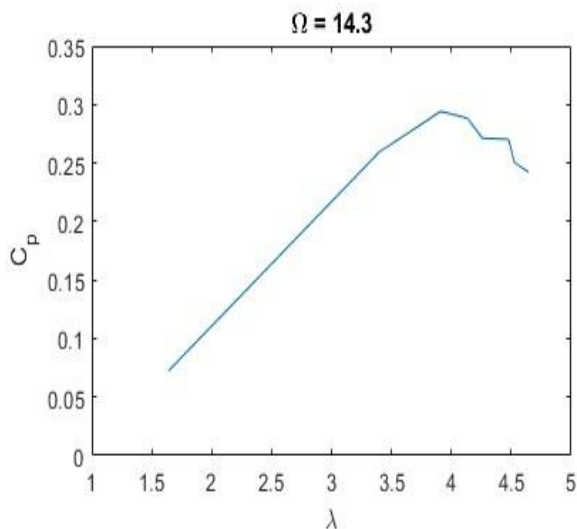


Figure 5: Tip speed ratio vs Coefficient of power

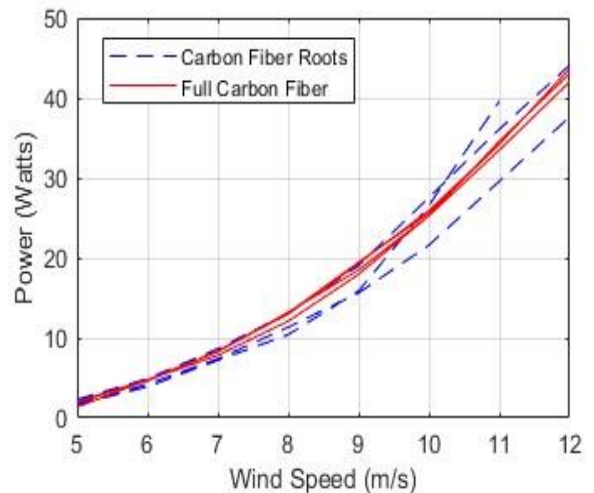


Figure 6: Carbon fiber roots vs full carbon fiber.

Pitch Control

The purpose of the pitch control system is to change the angle of attack of the blades to control turbine rotation speed, and drag force produced by the blades. The design focused on reducing the size and weight of the system and eliminating backdriving issues experienced with last year's design. Maintaining a high speed and accuracy in the system, and simplifying controls were also targets for the pitch control design process.

As seen in Figure 7, an Actuonix L16 linear actuator is used to move the swashplate along the driveshaft. The swashplate is fastened to the linkage plate through a radial ball bearing, which allows the linkage plate to rotate with the driveshaft. The linear movement of the linkage plate controls the

orientation of three curved linkage bars. These linkages connect to three blade collars, which rotate the blades to the desired angle of attack. A linear bearing and motion shaft fastened to the swashplate provide additional support to the cantilevered swashplate and linkage plate assembly. The linkage plate, linkages, and blade collars are machined from 6061 aluminum. Fasteners are alloy steel, and ball bearing carriages and balls are steel. The team controls the linear actuator through PWM control during competition and through the use of the Linear Actuator Control or LAC board during testing. The team found different pitch angles for cut-in and power and kept the PWM percent on as defined variables to be easily called.

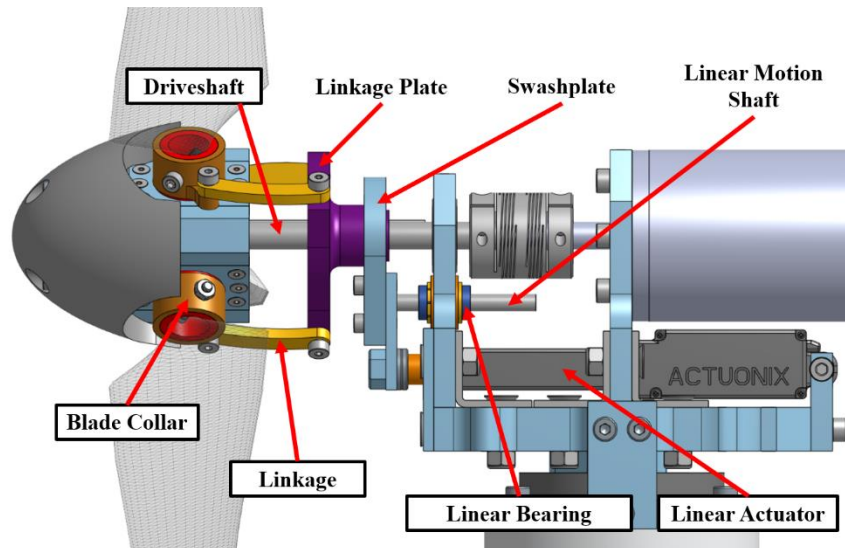


Figure 7: Pitch Control Diagram

The Actuonix L16 linear actuator was chosen due to its compact size, speed, accuracy, and good backdriving resistance. The L16 linear actuator was also an improvement in terms of how it was controlled from previous years use of a stepper motor. With the linear actuator the pitch angle was set by PWM rather than having to have the stepper motor mechanically set to zero introducing human error as well as increasing set-up time. The linkage and swashplate concept from last year has been re-used due to its simplicity and reliability; however, every part of the system has been redesigned and downsized to reduce size and weight (See Table 2).

Table 2: Quantification of Pitch Control Improvements

Competition Year	2022-23	2023-24
Actuation Distance (mm)	42.43	22.6
Volume of Actuation Components (cm ³)	467	93
Accuracy (Degrees)	5	1.98
Pitch Speed (Degree/s)	103	127

Blade Hub

The blade hub holds the blades and allows them to be rotated by the pitch control. The main goal of hub design this year was increasing the allowable blade length in order to produce more thrust, and decreasing hub weight in order to lower cut-in speed. Figure 8 shows a cross sectional view of the hub. The blades are mounted as close as possible to the driveshaft, in order to maximize blade length. The blade holsters are held in place by the bearing labeled in Figure 8. This is a captive ball bearing that is held in

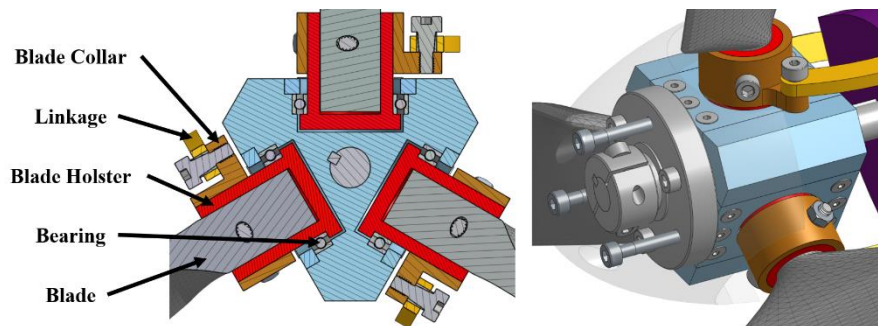


Figure 8: Left: hub cross section, Right: hub isometric view

place by an aluminum plate. This both reduces friction in the actuation and helps keep the entire assembly compact. To connect the blades to the pitch linkages, a collar is fitted around the blade holster and is held in place by the same pin that holds the blades in place (Figure 8)

A rapid prototyping process was used for the hub design with multiple 3D printed prototypes used for preliminary testing. The iterations of hub design are shown in Figure 9.



Figure 9: Top left: 2022-23 hub, Bottom right: 2023-24 hub

The final hub design was machined out of aluminum due to warping observed in some of the 3D printed prototypes at high rpm during durability testing. The aluminum hub and pitch control components have been tested up to 3900 rpm which is nearly twice the rotational speed the turbine will see in normal operation during competition. The new hub design has increased the allowable blade length by 31.6%, and decreased weight by 64.7% compared with last year's design.

Turbine Structures

The turbine's mounting structures connect the pitch control, drive shaft, generator, and nacelle to the tower. The design process started by identifying improvements that could be made to last year's design. With large reductions in size being made to the pitch control, the turbine's mounting structures also had to be reduced in size.

Throughout the design process, the turbine's mounting structures had small design changes to account for different pitch control methods; however, the general layout of the baseplate remained the same as presented in Figure 10.

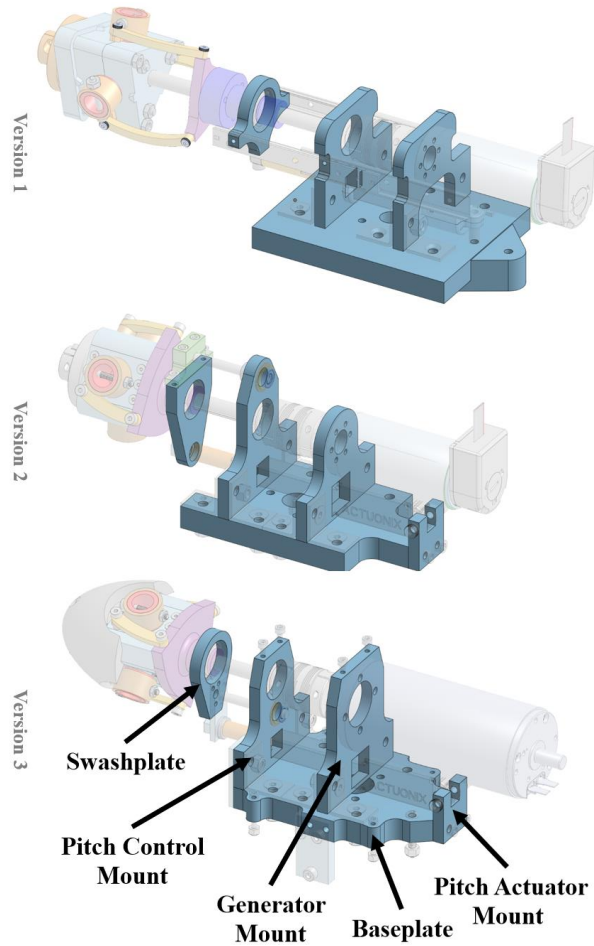


Figure 10: Evolution of baseplate and mounting plate

All of the mounting structures are machined from 6061 aluminum, the baseplate is 0.5” thick, and the swashplate, pitch control mount, generator mount, and pitch actuator mount are 0.25” thick (Figure 10). The pitch control mount and generator mount are connected to the baseplate through 0.08” thick 304 stainless steel brackets. Alloy steel bolts, lock-nuts, and threaded holes in the baseplate are used to fasten all parts together.

Yaw and Nacelle

The turbine uses a bearing and set screw to set yaw orientation (Figure 11). The bearing allows the turbine to be rotated into the wind direction, and the set screw is used to fasten the turbine in place before the wind tunnel is turned on.

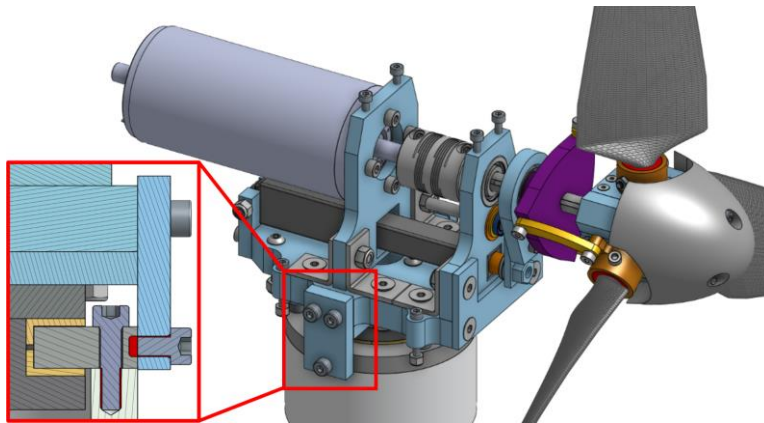


Figure 11: Set screw location and cross section.

The set screw design was validated during wind tunnel testing and showed no signs of movement during power generation and durability testing up to 22 m/s.

The nacelle is designed to fully enclose the turbine’s generator and pitch control mechanisms and reduce drag forces produced by these components. The nacelle is made from 3D printed PLA plastic and is fastened together using threaded heat set inserts.

Foundation

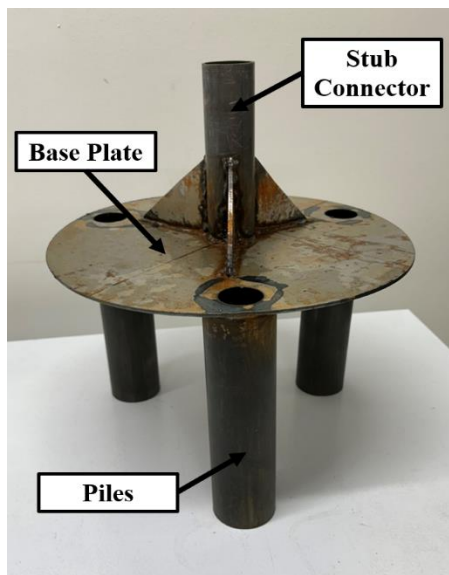


Figure 12: Wind turbine foundation

Design and Construction

The goal of the foundation is to secure the turbine in the simulation tank during testing, with minimal horizontal deflection. The tripod pile concept from last year is still being used, due to its promising strength to weight ratio; however, material thickness and pile diameters have been optimized to reduce weight while improving strength. The design consists of three 20 cm length, 2” OD tubes welded to a 30 cm diameter base plate (Figure 12). The connection tube for the stub is 1.5” OD and 16 cm long, it is supported by three 7 cm x 7 cm gusset supports (Figure 12). The foundation base plate and gussets are constructed entirely of 0.125” thick 4130 steel, the piles and stub connector are 0.058” thick 4130 steel (Figure 12). E71T-GS mild steel gasless flux core welding filament is used to fasten parts together. The foundation is designed so that the circular base plate sits flush on the top of the sand in the simulation tank (Figure 12).

Testing

Base plate size and pile diameter were optimized through testing. Base plate size was reduced by removing material from the center of the baseplate because the force provided by the sand interaction with the material along the edges of the circular foundation provides the longest moment arm and therefore the largest holding force. Base plates with 100%, 75%, 50%, and 25% mass (percentage of a full 29cm diameter baseplate) were tested (Figure 13).



Figure 13: 50%, 75%, and 100% base plates

Pile sizes of 2", 1.75", 1.5", and 1.25" OD were tested along with the various baseplate sizes. A modular construction method was developed to allow for rapid testing (Figure 14).

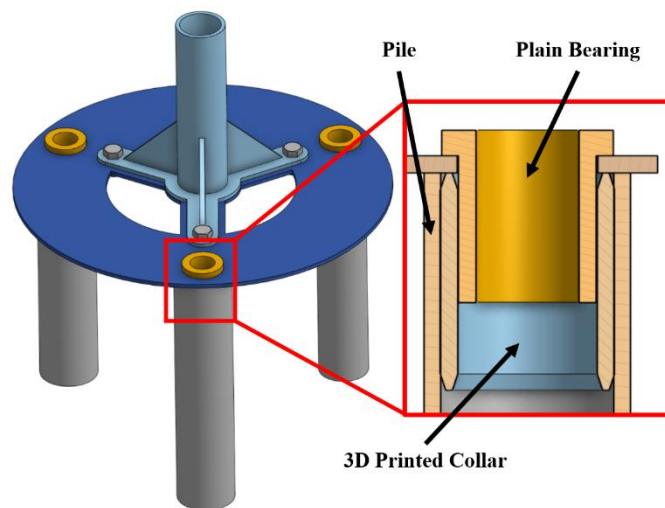


Figure 14: Modular testing foundation assembly

Piles were fastened to the base plate using flanged plain bearings press fitted into the piles using 3D printed collars (Figure 14). A bolt mounted stub connection piece was used to connect foundations to the stub and tower (Figure 14).

Testing was done in the team's lab space using the setup shown in Figure 15. Force and displacement measurements were recorded as each foundation was incrementally loaded until displacement passed 25 mm.

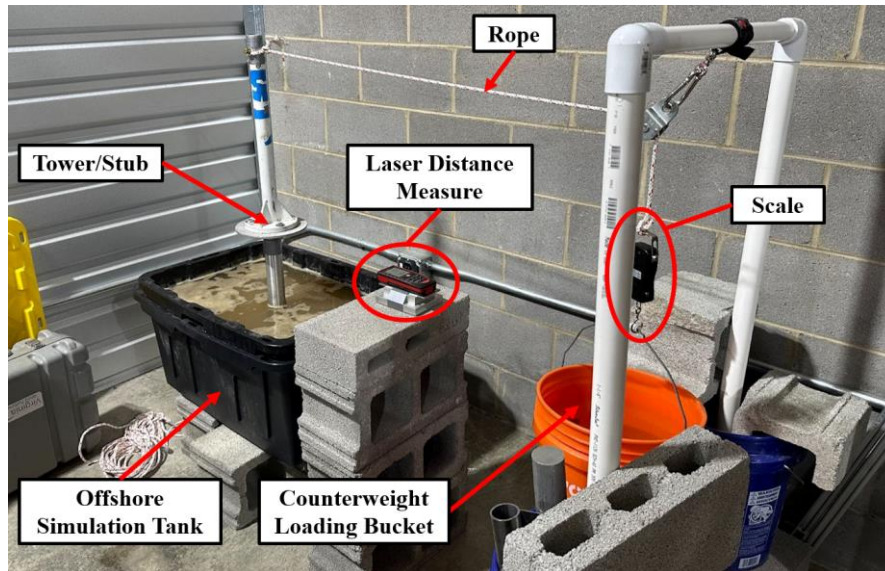


Figure 15: Lab testing setup

Force measurements from the lab testing setup were plotted against the maximum force on the turbine, and maximum allowable deflection (see Figure 16). The maximum wind force on the turbine was calculated experimentally by recording force vs deflection data in the lab, and wind speed vs deflection data in the wind tunnel for the same foundation. The maximum deflection from the wind speed vs deflection data set was aligned with an equal deflection value in the force vs deflection data set, the corresponding force in the force vs deflection data set was then recorded as the maximum wind force. This process was repeated 3 times for two different foundations, and an average value of 41.2 N, was determined as the maximum wind force. Figure 16 shows testing results for the foundation sizes tested.

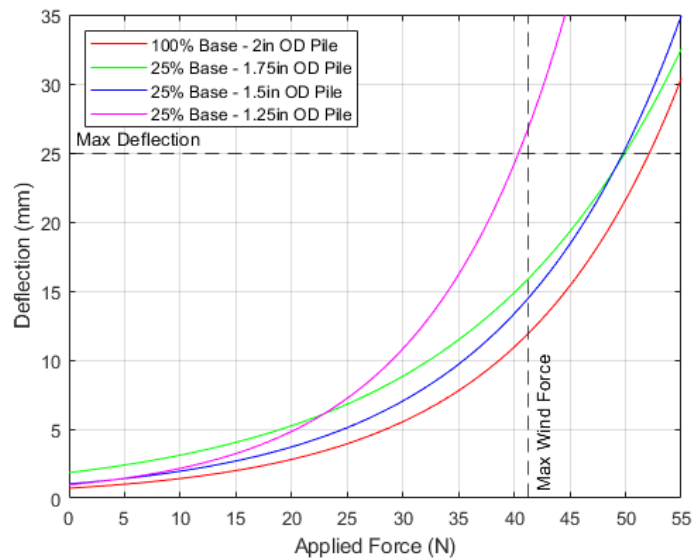


Figure 16: Foundation testing results

Based on this testing method a foundation with 100% baseplate and 2" OD piles was chosen, resulting in an experimental factor of safety of 1.2. The dry weight of this foundation was measured as 3.2 kg. The foundation was tested again in the wind tunnel during a full run through of all competition tasks to confirm its function.

Installation

The team identified foundation installation as another area for improvement. In previous years a hammer was used to drive the foundation into the simulation tank. This method was tedious and damaged the foundation, leading to failure in last year's structure. This year, a palm sander with a 3D printed attachment is being used to install the foundation (Figure 17).



Figure 17: Palm sander installation method being used to install foundation

The vibration of the palm sander is transmitted through the foundation and liquifies the sand surrounding the foundation, allowing it to slide into the sand quickly. This new method was inspired by the method used by JMU members last year. The vibration installation method takes about 30 seconds, while last year's method took 5 minutes.

Digitally Controllable Load

The Digitally Controllable Load (DCL) is designed to vary resistance to obtain maximum power output at every wind speed while ensuring safe operation with a resistance always in the load. The DCL is composed of four 2N7000 MOSFETS connected in parallel as voltage-controlled switches. Before using 4 2N7000 MOSFETS, the team used 1 IFRZ44N power MOSFET, but that MOSFET couldn't survive continuous operation. Relays were considered for the switching mechanism, but they would have led to size issues when putting the entire load side circuit together.

In the initial design, Arduino R4's were used to read the voltage coming from the turbine, and then begin supplying voltage to the gate. This presented a challenge, as the Arduinos could only output a maximum of three volts. For all the MOSFETS to leave the cut-off region, they needed a higher gate voltage from the Arduino. To amplify the voltage being supplied by the Arduino, boost converters set to 10V+ were implemented in series to the gates of the MOSFETS. Boost converters were used for the input of the MOSFET gate due to the high gate resistance of the MOSFET. Adding these components allowed for the MOSFETS to all be in saturation and act like ideal switches.

During testing, the team found that the MOSFETS weren't ideal switches and had some internal resistance when using the devices in saturation. On average, the parasitic resistance was about two to three ohms. Throughout testing without the DCLs being used, a resistance value of 20 ohms was found to be a good baseline resistor value. Using this 20-ohm resistance as a baseline, MOSFET switches with attached resistors were put in parallel to allow for a range of 9 ohms to 14 ohms of resistance that could be selected from to maximize the power output.

Having the resistors in parallel has the double benefit of heat reduction and ensuring that if any MOSFETs break there is always a fallback resistor that will prevent turbine run away.

Generator

The team narrowed the selection for the wind turbine's generator to two options: the Maxon RE 35 rated at 90 Watts and the Maxon RE 50 rated at 200 Watts. The former provided the team with an overall design approach centered on maximizing the system's power generation at lower wind speeds by choosing a smaller generator with lower internal resistance such that the turbine would cut in faster. The latter: however, gave the option to maximize power generation at higher wind speeds by choosing a larger generator that wouldn't cut in as quickly.

The Maxon RE 35 has a torque constant of 68 mNm/A and speed constant of 140 rpm/V, leading to a speed/torque gradient of 7.55 rpm/mNm. With a higher RPM at a smaller force, using this generator would theoretically provide the team with greater leeway at lower wind speeds, where the smaller torque from the spinning blades could be compensated for by having a faster spinning generator. Given that power generation at lower wind speeds is weighted higher in competition, this was the original generator of choice.

The Maxon RE 50 has a torque constant of 93.4 mNm/A and speed constant of 102 rpm/V, leading to a speed/torque gradient of 0.666 rpm/mNm. Given its lower speed constant and therefore lower RPM, it could be slowed more easily during emergency stop tests and lead to a safer system overall. Additionally, the smaller gradient value when compared to the RE 35 indicates that the RE 50 is better suited to produce more power but would spin slower at low wind speeds and therefore reduce the point potential at those speeds.

Performing multiple trials in testing with a wind tunnel, the team calculated the estimated score that would be received at competition with each generator at wind speeds varying between approximately 5 m/s and 11 m/s, incrementing by ~1 m/s for each test. The average results for this testing between two separate trials for the RE 35 generator is seen below:

Table 3: Estimated CWC Points for Varying Wind Speeds for RE 35 and 50 Generators

RE 35 Generator		RE 50 Generator	
Wind Speed (m/s)	CWC Points (Average)	Wind Speed (m/s)	CWC Points (Average)
5.01	1.12	5.01	0.33
6.01	2.35	6.01	1.45
6.98	4.08	6.98	4.75
8.02	5.39	8.02	8.58
9.03	4.23	9.03	7.35
10	4.09	10	7.56
10.99	1.85	10.99	3.38
TOTAL:	23.12	TOTAL:	33.40

Table 3 displays these average results between two separate trials for the RE 50 generator. It was found that the RE 35 generator is more effective at low wind speeds. Results from testing show that points were between approximately 0.7 and 0.9 higher than that of the RE 50 between ~5 and ~7 m/s. However, for every wind speed thereafter, the total points increased by a significantly larger margin for the RE 50 generator, culminating in approximately 10.3 more points overall when compared to the RE 35's total. Therefore, despite lower wind speeds being more heavily weighted in competition, the team

saw it more effective to utilize a larger generator to capitalize on the larger point gains at wind speeds at or above 8 m/s.

Turbine Side Electronics

This year, the control systems integrated an Arduino R4 at the turbine side. The microcontroller is tasked with the responsibility of overseeing the linear actuator, which in turn is responsible for the pitch of the blades. The linear actuator is powered and controlled by the turbine-side microcontroller and controlled by using the finite-state machine logic (see figure 18). The coordination between the turbine-side and load-side subsystems was streamlined by using an optocoupler, which allowed for UART communication. The UART communication allows for the DCL to tell the turbine-side the current voltage being produced, allowing for the FSM logic to work. For a comprehensive, one-line diagram of the subsystems, refer to Figure 18 below.

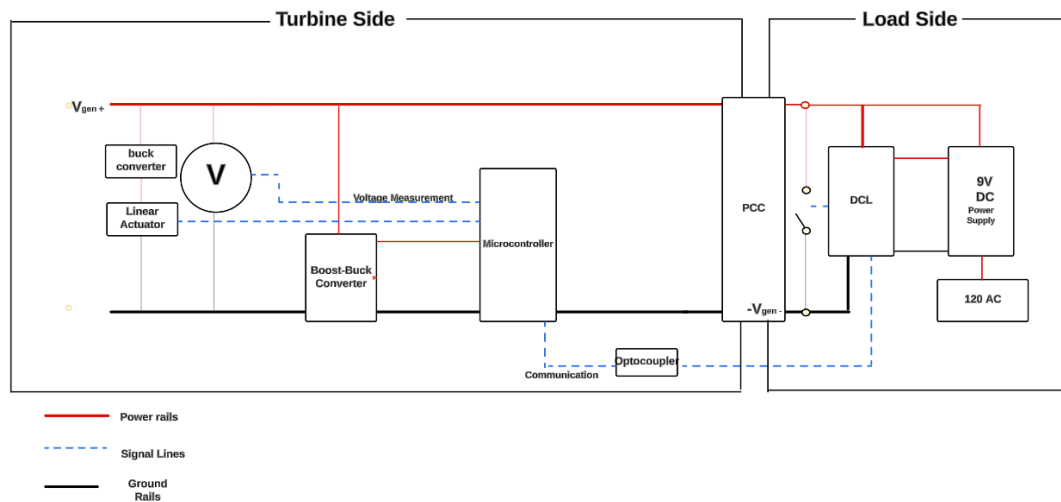


Figure 18: One-line diagram of electrical subsystems

Finite State Machine

The Finite State Machine (FSM) plays an intricate part in the control system. It consists of five primary states: Cut-In, Power, Rated Power, Durability, and Safety, each making the turbine function differently to ensure that the CWC Requirements are met. The Finite State Machine Diagram is shown in Figure 19. The Cut-In state represents the state in which the turbine is activated from a stationary state, meaning it is optimized for low wind speeds. This is the initial state of the turbine, so when the turbine is starting up, or coming out of safety, this is the state that is active. The Power state is the state in which the turbine is positioned for the highest power transfer possible, at wind speeds approximately between 5 - 11 m/s. This state is activated when the voltage threshold is reached from the Cut-In state. Rated Power is the mode aptly named for the rated power task that keeps the turbine power at its rated power at wind speeds of 12, 13 and 14m/s. The durability state represents the turbine operation at high wind speeds, with a focus on minimizing load and preventing runaway. If the voltage produced is higher than the durability voltage chosen, and the turbine pitch is less than 100%, then the durability state is activated. The final state is the Safety state, which may be activated in two ways: either through a button press or load disconnect. Either way, this activates the safety state, which causes the turbine to come to a complete stop and prepares the electronics to shut down. When the safety button is released, or load is reconnected, the FSM restarts, with an initial Cut-In state once again. Depending on whichever state the Load-Side FSM is in, it will also send a UART Signal through the optocoupler to the turbine side, allowing the turbine-side controls to adjust the pitch as needed, as well as any other turbine side parts, such as the voltage measurement. The FSM for the turbine side can be seen in Figure 20.

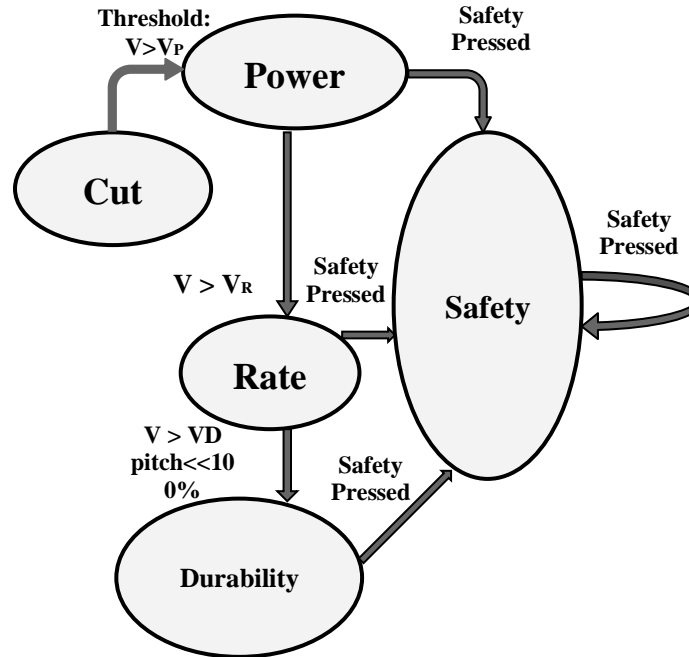


Figure 19: Load-Side Finite-State Machine Diagram

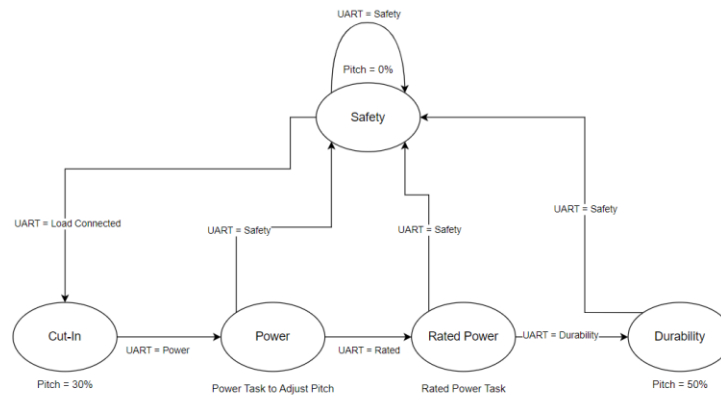


Figure 20: Turbine-Side Finite-State Machine Diagram

Use of Legacy Parts

Part	Description of Re-use
Yaw Bearing	The team found that the bearing and mount used last year were still functional, and changes to their design would not result in any performance increase. The team decided to instead dedicate time to changing parts of the turbine that would result in improvements in turbine performance.
Yaw Bearing Mount	
Generator	See <i>Generator</i> section

References

- [1] Airfoils at low speeds, https://m-selig.ae.illinois.edu/uiuc_lsai/Airfoils-at-Low-Speeds.pdf (accessed Oct. 19, 2023).
- [2] Summary of low-speed airfoil data, https://m-selig.ae.illinois.edu/uiuc_lsai/Low-Speed-Airfoil-Data-V1.pdf (accessed Sep. 22, 2023).
- [3] R. K. Singh, M. R. Ahmed, M. A. Zullah, and Y.-H. Lee, “Design of a low Reynolds number airfoil for small horizontal axis wind turbines,” ScienceDirect, <https://www.sciencedirect.com/science/article/pii/S0960148111005325> (accessed Oct. 3, 2023).
- [4] Momentum Theory, https://www3.nd.edu/~tcorke/w.WindTurbineCourse/Aerodynamics_Presentation.pdf (accessed Oct. 10, 2023).